DD

KEK Preprint 94-105
September 1994
H

A Beam Test of a Calorimeter Prototype of PWO Crystals at Energies between 0.5 and 2.5 GeV

S. Inaba[a)], M. Kobayashi[a)], M. Nakagawa[b)], T. Nakagawa[c)], H. Shimizu[d)], K. Takamatsu[a)], T. Tsuru[a)] and Y. Yasu[a)].

[a] *National Laboratory for High Energy Physics (KEK), Tsukuba, Ibaraki 305, Japan*
[b] *Miyazaki University, Gakuen-Kihanadai-Nishi, Miyazaki, 889-21, Japan*
[c] *Tohoku University, Aoba, Sendai 980, Japan*
[d] *Yamagata University, Kojirakawa, Yamagata 990, Japan*

Abstract

Results of a beam test are presented on energy resolutions of a calorimeter hodoscope prototype of PWO ($PbWO_4$) crystals, measured by electron beams with energies between 0.5 and 2.5 GeV. The hodoscope is consisted of a 3 x 3 matrix of modules of a PWO which has dimensions of 20 mm x 20 mm in cross section and 200 mm in length. An energy dependence of energy resolutions is obtained to be $(\sigma/E(GeV))^2 = ((0.0310 \pm 0.0011)/\sqrt{E(GeV)})^2 + (0.0079 \pm 0.0025)^2$ fitted by the quadratic form.

Submitted to Nuclear Instruments and Methods A.

National Laboratory for High Energy Physics, 1994

KEK Reports are available from:

Technical Information & Library
National Laboratory for High Energy Physics
1-1 Oho, Tsukuba-shi
Ibaraki-ken, 305
JAPAN

Phone: 0298-64-1171
Telex: 3652-534 (Domestic)
(0)3652-534 (International)
Fax: 0298-64-4604
Cable: KEK OHO
E-mail: LIBRARY@JPNKEKVX (Bitnet Address)
library@kekvax.kek.jp (Internet Address)

A Beam Test of a Calorimeter Prototype of PWO Crystals at Energies between 0.5 and 2.5 GeV

S. Inaba[a)], M. Kobayashi[a)], M. Nakagawa[b)], T. Nakagawa[c)], H. Shimizu[d)], K. Takamatsu[a)], T. Tsuru[a)] and Y. Yasu[a)].

[a] *National Laboratory for High Energy Physics (KEK), Tsukuba, Ibaraki 305, Japan*
[b] *Miyazaki University, Gakuen-Kihanadai-Nishi, Miyazaki, 889-21, Japan*
[c] *Tohoku University, Aoba, Sendai 980, Japan*
[d] *Yamagata University, Kojirakawa, Yamagata 990, Japan*

A heavy crystal, PWO ($PbWO_4$) which emits scintillation lights, has been highly expected to be used for a radiator of EM-calorimeters (1-5). The chemical and physical properties of it are stable and scintillation lights have an emission peak around 500 nm with a fast decay time constant less than 20 ns. An amount of scintillation lights is estimated to be 10% of BGO at most. PWO will be an excellent radiator at high energy. We may expect it will be useful at lower energy, as well. Recently, characteristics of a hodoscope prototype have been studied in the energy range between 10 and 100 GeV of the incident electrons at CERN (6). It will be important to study characteristics of a PWO hodoscope at lower energies, in order to see parameters for energy resolution of calorimeter hodoscopes precisely.

We have measured energy resolutions of a calorimeter hodoscope prototype of a 3 x 3 matrix of PWO modules viewed by photomultiplier tubes. The PWO module had a shape of rectangular parallelepiped with 20 mm x 20 mm in cross section and 200 mm in length. Surfaces of it were polished. The hodoscope was irradiated by electron beams with energies between 0.5 and 2.5 GeV. We report here results of the studies on energy resolutions measured on the hodoscope prototype.

The PWO crystals were produced at RI&NC (7) in Minsk. A typical transmission curve and excitation and emission spectra of the PWO are shown in Fig. 1 for a sample of 2.0 x 2.0 x 1.3 cm^3 which has been prepared from the same ingot for the module. Transmission curves and emission spectra have no sizable difference among the modules. Though nine crystals have been grown up under the same condition, the three modules out of nine have lengths of 180 mm depending on growing processes. These three were arranged at the corners of the 3 x 3 matrix. Electron beams hit upon the hodoscope along the long axis of the PWO. The PWO crystal was wrapped by aluminized Mylar sheet at side surfaces along the long axis. A Milpore sheet was put on a square surface opposite to that viewed by the PMT. The type, R4125 of

Hamamatsu (19 mm dia. with 15 mm dia. of photocathode of extended green bialkali) was chosen as a photon sensor. Silicon grease of DawCorning Q2-3067 (refractive index, n = 1.5) was used between the crystal and the PMT for the optical coupling. The hodoscope prototype was housed in an aluminum case for light shield. The electron beams hit the hodoscope through an aluminum plate with 0.5 mm thick at the window of the case. Output signals from PMT's were transferred to ADC's (LeCroy 2249W) via 5D-2V cables with 30 m in length.

The aluminum case was not taken care of for temperature fluctuations at this time. A sizable amount of temperature dependence (about -2% / °C) has been reported (8) for the light output of PWO crystals. We took care to use only the data taken during the late of evening and the night when temperature fluctuation might be small relatively. We may expect to have less effect from temperature fluctuation by choosing the time for the data taking. We estimate our data have been collected under the condition of the temperature variation in our experimental hall within ±1 °C.

Electrons were produced at the internal target of the 12 GeV PS at KEK. They were transported through the π2 beam line and the π2-B beam line at the downstream of it to the hodoscope prototype as shown in Fig. 2(a). The tracking chamber system on the π2-B line is composed of four sets of X and X' (staggered by a half cell size) for the horizontal coordinate and two sets of Y and Y', i.e. X_1X_1', Y_2Y_2' and X_3X_3' at the upstream of the magnet, 8D240 and X_4X_4', Y_5Y_5' and X_6X_6' at the downstream of it. A finger counter, F(10), with a size of 10 mm x 10 mm was used in front of the hodoscope prototype to localize a beam onto a single module of the hodoscope. The two gas Cerenkov counters, C_1 and C_2, filled with CO_2 gas were used for the identification of electrons in the beam at 1.34 and 1.30 atmospheric pressure, respectively. The schematic layout of the π2-B beam line is shown in Fig. 2(b). The beam tracking has been done for the X-coordinates of the chambers at the upstream of the magnet and for those at the downstream independently and for the Y-coordinates through the upstream and the downstream together for the beam defined by the counters, S_1, S_2, S_3 and F(10). The momentum has been determined by the deflection angle between the tracks of the upstream and the downstream. A He bag was used between the chambers at the upstream and the downstream to minimize effects of multiple scattering. A typical distribution of the beam momentum is shown for the electron beam of 1 GeV/c in Fig. 3. The momentum resolution of the beam, σ_{beam}/p, has been obtained to be $(0.805 \pm 0.019)\%$ at 1 GeV/c by Gaussian fitting.

The calibration for relative gains of nine modules of the PWO was done module by module irradiated by the pion beam of 2.0 GeV/c. High voltage values for PMT's were arranged so that the dynamic range of the ADC met the energy range of the electron beams up to

2.5 GeV. The values of calibration factors have been determined with accuracy in the range between 0.3 and 0.5%.

A longitudinal uniformity of the crystal was examined by the pion beam of 2 GeV/c irradiated perpendicularly to the longitudinal axis of the crystal. A PWO of 20 mm x 20 mm x 168 mm in sizes was viewed by a 2" PMT of Type R1181 of Hamamatsu. A sheet of white paper was put on the surface of the opposite side to the PMT as a reflector. Side surfaces were wrapped by aluminized Mylar sheet. The optical coupling was arranged by using the DawCorning Q2-3067 grease between the crystal and the PMT. The pion beam was defined by the F(10) finger counter put in front of the crystal. A typical signal distribution is shown for the deposit energies measured at the center along the longitudinal axis, as an example, in the figure inserted in Fig. 4, where peak positions of deposit energies are plotted with respect to the distances from the photocathode of the PMT. We can see a flat response in the region around the center of the crystal and far from the photocathode, but rather higher acceptances near to the photocathode. The larger area of the photocathode than the cross section of the crystal may explain them.

EM-shower signals have been measured by the hodoscope prototype at 0.5, 1.0, 1.5 and 2.5 GeV of electron energies. The profile of the electron beam was defined by the finger counter, F(10), put just in front of the #5 module which was set at the center of the hodoscope prototype. Events were triggered by the logic, $S_1 \cdot S_2 \cdot S_3 \cdot C_1 \cdot C_2 \cdot F(10)$. Fig. 5 shows energy distributions on each module deposited by 1 GeV electrons. ADC values of signals were corrected by the pedestal subtraction and the energy calibration at the off-line analysis. Fig 6 shows the energy distribution of the sum of energies of all modules, #1 - #9, deposited by 1 GeV electrons on the hodoscope. The solid line in the figure shows the Gaussian curve which is well fitted to the distribution to extract energy resolution parameters.

Values of the observed energy resolution, σ_{obs}/E, of the hodoscope prototype are plotted with solid circles for electron energies, 0.5, 1.0, 1.5 and 2.5 GeV in Fig. 7. Error bars indicate statistical uncertainties in the fitting. They are also tabulated in the second column of Table 1 with the beam momentum resolutions, as well. Around 5,000 events were analyzed at each momentum of the beam. The energy resolution parameters are obtained by averaging values for every 1000 events analyzed in order that effects due to variation of temperature surrounding the hodoscope can be minimized. It took about half an hour to get 1,000 events depending on the electron energies. Temperature variation was estimated to be less than half degree during the measurement. All data shown were taken during the evening and night when temperature variation was small, comparatively. We collected data at 2.0 GeV of the electron beam as well, but they were, unfortunately, taken in day time when the room temperature was

higher than that in the evening and night by more than 5 degree. Though we may expect the resolution parameters are not affected much by the difference of temperature, we did not use the data at 2.0 GeV in our result and do not show them in the figure. Reader can refer the parameter values at 2.0 GeV in Table 1. Data at 2 GeV have been analyzed in the same manner as those at the other energies. The beam momentum resolution measured are plotted with open squares in the figure, as well.

The observed energy resolution, σ_{obs}/E, can be expressed by a quadratic sum of an uncertainty of the hodoscope, σ_{hodo}/E, and that due to the momentum resolution of the beam, σ_{beam}/E, i.e. $(\sigma_{obs}/E)^2 = (\sigma_{hodo}/E)^2 + (\sigma_{beam}/E)^2$. The values of σ_{hodo}/E are tabulated in the third column of Table 1 and are shown in Fig. 8 by solid circles with respect to $1/\sqrt{E}$. Considering that the energy resolution of calorimeters is parametrized (9) by the statistical term and the constant term, conventionally, and expressed by the quadratic sum of the two terms, as $(\sigma_{hodo}/E(GeV))^2 = (a/\sqrt{E(GeV)})^2 + b^2$, we have obtained $a = 0.0310 \pm 0.0011$ and $b = 0.0079 \pm 0.0025$. The solid line in the figure shows the result of the fitting. The result obtained at CERN(6) is consistent with ours.

We may extract an intrinsic energy resolution of the PWO, σ_{PWO}/E, if we can estimate fluctuations in the amount of leakage of energy deposit in the crystals reasonably. σ_{hodo} can be a quadratic sum of σ_{PWO} and σ_{leak}, as $(\sigma_{hodo}/E)^2 = (\sigma_{PWO}/E)^2 + (\sigma_{leak}/E)^2$, where σ_{leak} is a fluctuation of an energy leakage of an E-M shower from the PWO estimated by Monte Carlo calculation using the EGS4 code. We neglect effects from fluctuation of the energy deposited in the dead materials surrounding the crystals and those from collection or generation of the signal and others in the estimation. The values of σ_{leak}/E are plotted by open circles in Fig. 7 and are shown in Table 1. Values of σ_{PWO}/E are also tabulated in Table 1 and are plotted with open circles in Fig. 8. The dotted line in the figure is the curve fitted by $(\sigma_{PWO}/E(GeV))^2 = (a'/\sqrt{E(GeV)})^2 + b'^2$ with $a' = 0.027 \pm 0.0012$ and $b' = 0.0027 \pm 0.0070$.

We can estimate a photoelectron number from the parameter, a', which accounts for the statistical fluctuation in the number of photoelectrons converted by the photosensors. The number of photoelectrons is estimated to be 1.4 MeV^{-1} for the extended green photocathode of the Hamamatsu's PMT with photon collection efficiency of 0.44.

The e / π rejection has been examined with use of the pion beams at the same conditions as those for the electrons except for Cerenkov counters in the trigger logic. No Cerenkov counter was used for the beam trigger. The distribution of energies deposited on the hodoscope by the 1 GeV/c negative beam is shown in Fig. 9(a). We can see a sharp peak around 250 MeV corresponding to the ionization loss of pions on a broad bump due to the nuclear interactions of the negative pions. A clear peak due to the electrons is also seen at the position. Taking a

criterion that events which has deposit energies in the range, $\pm 2\sigma$ (σ = 26.4 MeV at 1.0 GeV) around the electron peak should be electrons, we can estimate a rejection factor, a number of fake electrons produced by a negative pion. Extrapolating the curve fitted by the exponential form, ce^{-kE} around higher energy tail of energy deposit excluding the electron peak, we estimate the number of events in the electron region, $\pm 2\sigma$ at the electron peak. Details of the energy deposit at the higher energies with the curve fitted are shown in the logarithmic scale in Fig. 9(b). A rejection factor is obtained to be $1.18 \, ^{+0.48}_{-0.34} \times 10^{-3}$ for the negative pions of 1.0 GeV. Those for 0.5, 1.5 and 2.5 GeV are obtained in the same manner of the estimation, as shown in Fig. 10. A level of 2×10^{-3} of a rejection factor is attainable with the hodoscope at lower energies around 1 – 2 GeV.

In summary, we have measured energy resolutions of the calorimeter hodoscope prototype of PWO crystals with the electron beam of energies between 0.5 and 2.5 GeV. The hodoscope is consisted of the 3 x 3 matrix of PWO crystals. The crystal has dimensions of 20 mm x 20 mm x 200 mm. The energy dependence of the energy resolutions is parametrized by the quadratic form to be $(\sigma/E(GeV))^2 = ((0.0310 \pm 0.0011)/\sqrt{E(GeV)})^2 + (0.0079 \pm 0.0025)^2$ fitted. The photoelectron number is estimated for the PWO to be 1.4 MeV^{-1} with the photomultiplier tube of the extended green photocathode of the type R4125 of Hamamatsu. The PWO crystal is an excellent material for total absorption E-M calorimeters at high energies at the following points, the fast decay time of signal, the reasonable energy resolution, the high resistivity for radiations and the stable characteristics in physical and chemical properties. Taking the advantage of the fast decay time of signal, it will also be useful at lower energies. The e / π rejection of the hodoscope has been examined. The distribution of energy deposit of negative pions shows that a level of 2×10^{-3} for the e / π rejection is attainable with the hodoscope for the negative pion beam around 1 – 2 GeV.

Authors would thank the director general of KEK, Prof. H. Sugawara and the director of the physics department of KEK, Prof. S. Iwata for continuous encouragement and supports for the R&D studies on heavy crystals. They are also indebted to the kind arrangements of the PS division of KEK for the beam test at the 12 GeV proton synchrotron. Prof. M. Takasaki and Prof. M. Fukushima are deeply acknowledged for giving us details of information on the π2-B beam line which has been installed, recently. Authors are particularly indebted to Prof. M. Fukushima, Dr. N. Toomi and their colleagues of the B-physics project for the tracking procedures as well as the arrangements of the chamber system. Advice and encouragement of Professors, Yu.D. Prokoshkin, J.P. Stroot and J.P. Peigneux of the GAMS collaboration were invaluable. Stimulative discussions with and valuable information from Dr. M. Poulet, A.V. Singovsky, V.A. Kachanov, M. Korzhik and A.A. Fyodrov were fruitful and acknowledged. One of the authors, M. N, thanks Prof. T. Hasegawa and Dr. T. Matsuda who gave him guidance and encouragement during the studies.

References

1. Heavy scintillators, Proc. of the crystal 2000, Int. Workshop, Chamonix, France, Ed. De. Totristefani, P. Recoq, M. Schneegans, Frontieres, C58 (1993), Gif-sur-Yvette, France. Articles herein.
2. V.A. Baryshevsky et al., Nucl. Instr. Meth. A322 (1992) 231.
3. V.A. Kachanov et al., Beam studies of EM calorimeter prototype built of PWO crystals, reported on the IV Int. Conf. on Calorimetry in High Energy, Sep. 1993, Isola Elba, Italy.
4. M. Kobayashi et al., Nucl. Instr. Methods A333 (1993) 429.
5. V.A. Kachanov et al., Properties and beam test of $PbWO_4$ crystals, LAPP-EXP-93-08, to be published in the Proc. of IEEE 93 Nucl. Sci. Symposium, Nov. 1993, San Francisco, California.
6. O.B. Buyanov et al., A first electromagnetic calorimeter prototype of $PbWO_4$ crystals, LAPP-EXP/94-06 (1994).
7. Radiation Instruments and New Components Ltd., Minsk, Belarus.
8. G.H. Grayer, Internal report on properties of $PbWO_4$ scintillator and its use for LHC calorimetry, 1993.
9. T.S. Virdee, Performance and Limitations of Electromagnetic Calorimeters, Proc. the 2nd Int. Conf. on Calorimetry in High Energy Physics, Capri, Italy, Oct. 1991, Ed. Ereditano, World Scientific, Singapore, p.3.

Table caption

Table 1. Observed energy resolutions, (σ_{obs}/E), beam momentum resolutions (σ_{beam}/p) and fluctuation of E-M shower leakage (σ_{leak}/E) estimated by the EGS4 code at electron energies between 0.5 and 2.5 GeV. Energy resolutions of the hodoscope prototype(σ_{hodo}/E) and the intrinsic energy resolutions of the PWO (σ_{PWO}/E) are in the last column.

Figure captions

Fig. 1. Transmission curve and excitation and emission spectra of the PWO. The data were taken for the sample with thickness of 1.3 cm. The horizontal scale is arbitrary for excitation and emission.

Fig. 2. Schematic view of the $\pi 2$ and the $\pi 2$-A and -B lines (a) and the $\pi 2$-B beam line (b) at the 12 GeV PS. C_1 and C_2: gas Cerenkov counters, S_1 - S_3: trigger counters, F(10): finger counter, 8D240: analyzer magnet and DC: sets of drift chambers.

Fig. 3. Momentum spectrum of the beam at 1 GeV/c. Solid line shows the results of the Gaussian fitting.

Fig. 4. Longitudinal uniformity of the PWO crystal measured by the pion beam of 2 GeV irradiated perpendicularly to the longitudinal axis of the crystal. Distance is measured from the photocathode of PMT along the long axis of the crystal. Inserted is a typical distribution of the energy deposit measured at the center along the axis of the PWO, as an example.

Fig. 5. Observed energy deposit of 1 GeV electrons on the modules, #1-#9, of the hodoscope. The beam is defined by the trigger, $S_1 \cdot S_2 \cdot S_3 \cdot C_1 \cdot C_2 \cdot F(10)$. F(10) (10mm x 10mm) was located at the center of the #5 module. ADC values are corrected by pedestal subtraction and energy calibration.

Fig. 6. Energy distribution of the sum of the energies deposited on all modules of the hodoscope by the 1 GeV electrons. One fifth of the total events is plotted. Solid line is a curve fitted by Gaussian.

Fig. 7. Observed energy resolutions of the hodoscope (solid circles), fluctuations of the energy leakage of the E-M shower (open circles) in the hodoscope and beam momentum spreads (open squares).

Fig. 8. Energy resolutions of the hodoscope (solid circles) estimated from observed energy resolutions and momentum spreads of the beam. Open circles show the energy resolutions of the PWO estimated by energy resolutions of the hodoscope and fluctuations of the energy leakage. Curves are results of fitting with the quadratic sum of the statistical term and the constant one for the energy resolutions of the hodoscope (solid line) and the energy resolutions of PWO (dotted line).

Fig. 9. Energy deposit of the negatively charged beam of 1 GeV/c on the hodoscope (a). Deposit energies on the modules, #1-#9, are summed up. Details around the maximum energy deposit are shown (b) in the logarithmic scale for the event numbers. The pion tail at higher energy just before the maximum energy is fitted by the exponential curve (solid line) for the estimation of the number of fake electrons in the range, $\pm 2\sigma$ under the electron peak.

Fig. 10. e / π rejection factors estimated for negative pions.

Table 1.

Electron Energy (GeV)	σ_{obs}/E (%)	σ_{beam}/p (%)	σ_{leak}/E (%)	σ_{hodo}/E (%)	σ_{PWO}/E (%)
0.5	4.441 ±0.205	1.002 ±0.050	2.170 ±0.039	4.326 ±0.211	3.743 ±0.245
1.0	3.338 ±0.075	0.805 ±0.019	1.663 ±0.035	3.239 ±0.077	2.780 ±0.092
1.5	2.755 ±0.074	0.753 ±0.022	1.470 ±0.024	2.650 ±0.078	2.205 ±0.095
2.0	2.550 ±0.053	0.587 ±0.014	1.232 ±0.025	2.233 ±0.055	2.154 ±0.090
2.5	2.185 ±0.046	0.559 ±0.013	1.195 ±0.024	2.112 ±0.047	1.742 ±0.060

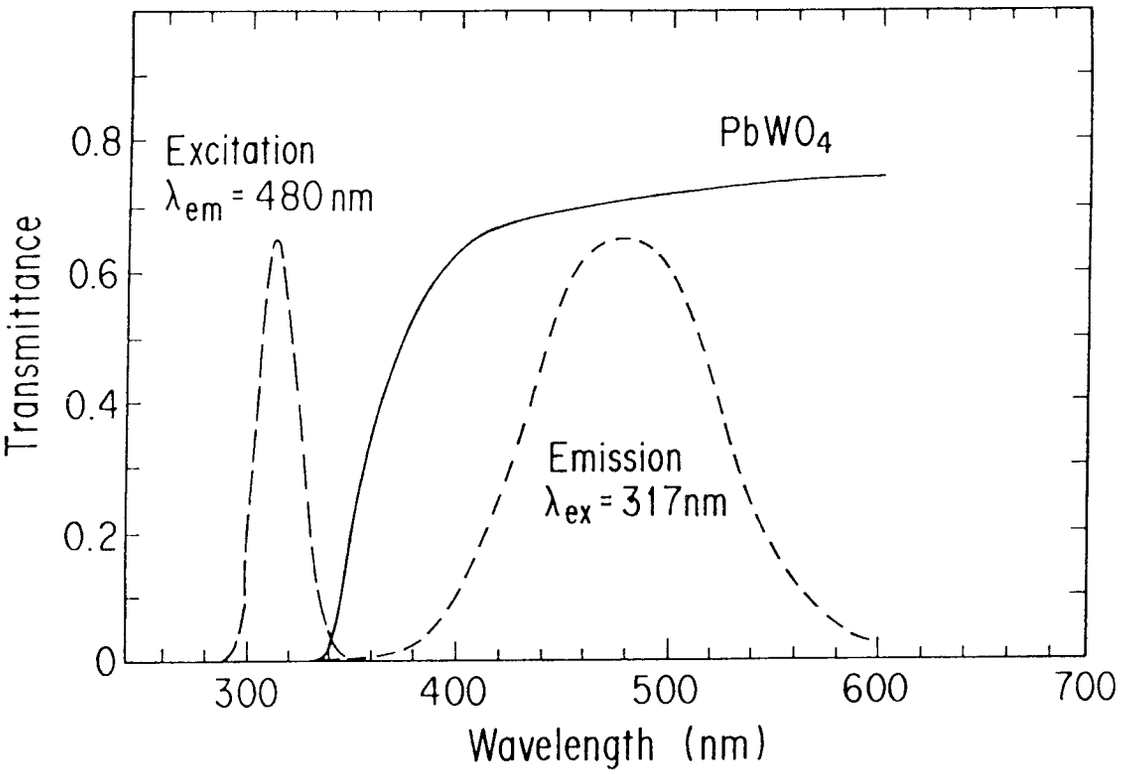
Excitation
λ_{em} = 480 nm
$PbWO_4$
Emission
λ_{ex} = 317nm
Transmittance
0.8
0.6
0.4
0.2
0
300
400
500
600
700
Wavelength (nm)

Fig. 1.

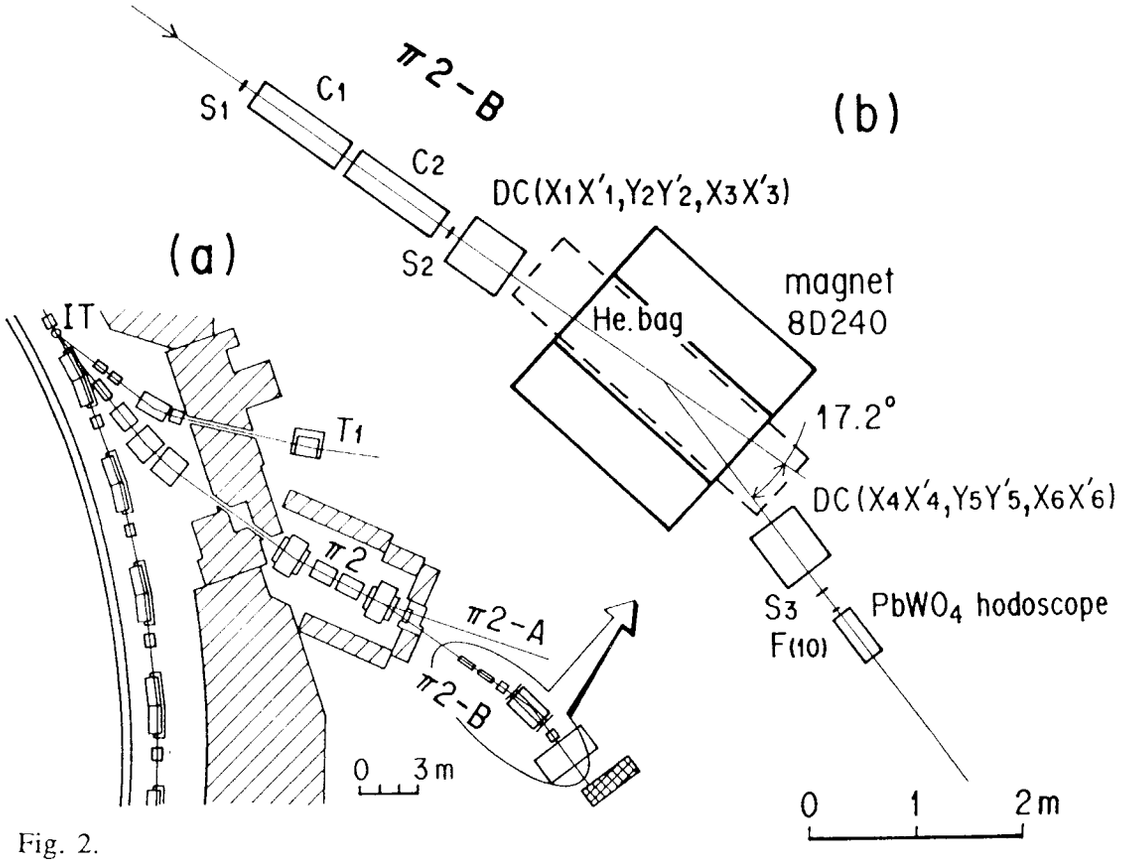
S1
C1
π2-B
C2
DC(X1X'1,Y2Y'2,X3X'3)
(b)
(a)
S2
magnet
8D240
He.bag
IT
T1
17.2°
DC(X4X'4,Y5Y'5,X6X'6)
π2
π2-A
S3
F(10)
PbWO4 hodoscope
π2-B
0 3m
0 1 2m

Fig. 2.

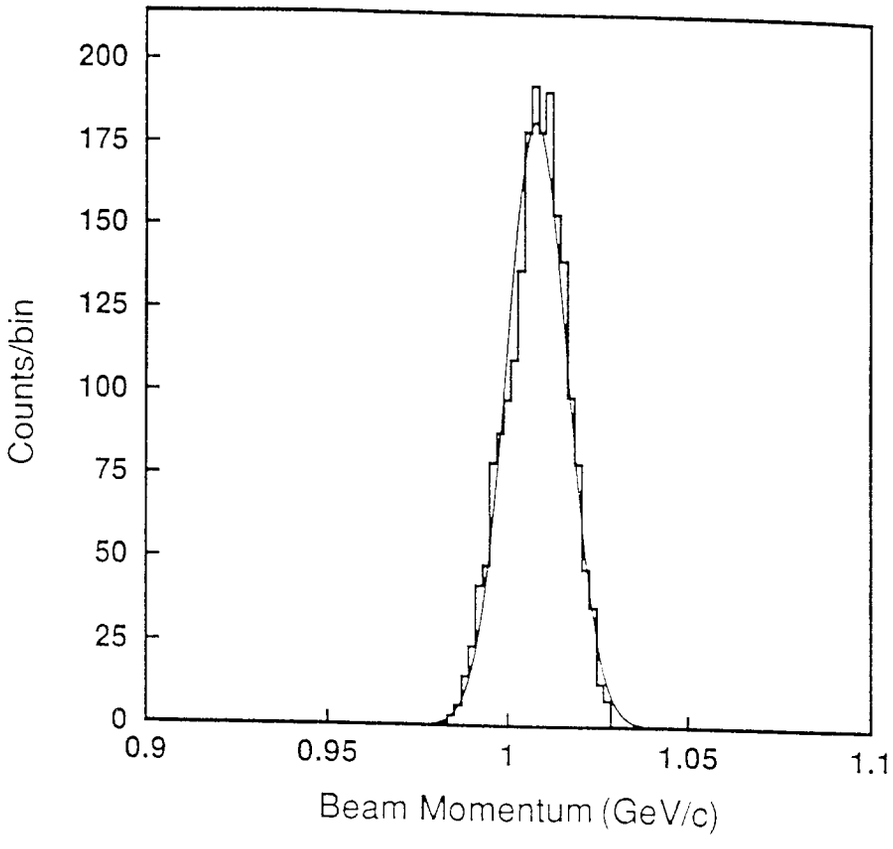
Counts/bin
200
175
150
125
100
75
50
25
0
0.9
0.95
1
1.05
1.1
Beam Momentum (GeV/c)

Fig. 3.

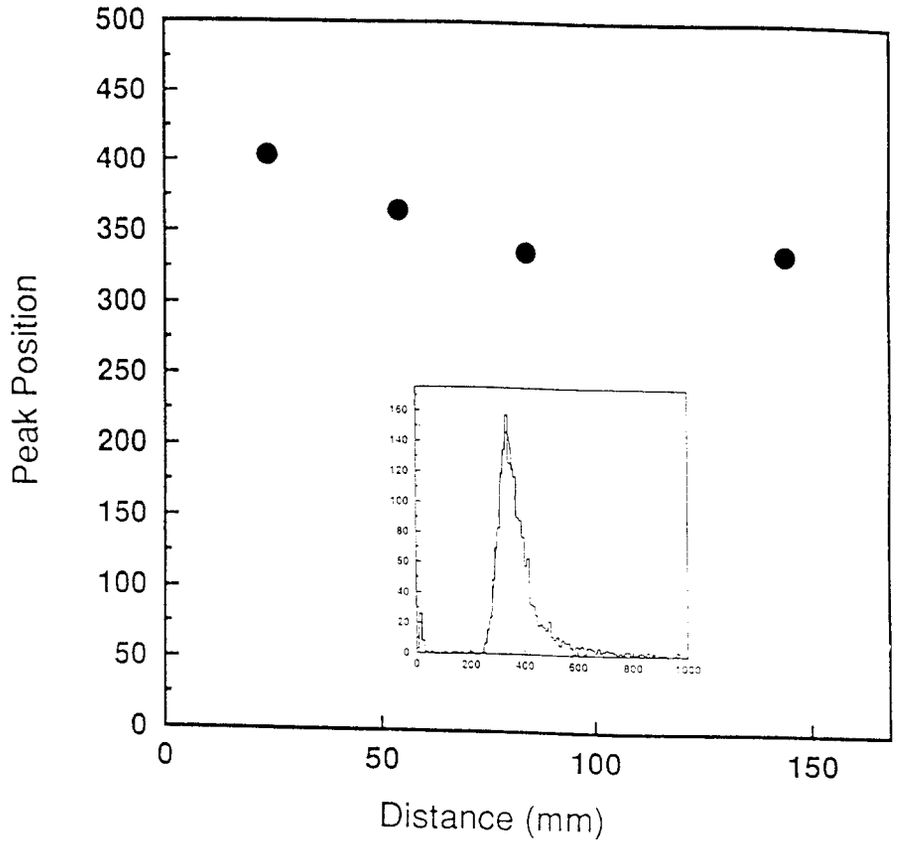
Peak Position
500
450
400
350
300
250
200
150
100
50
0
0
50
100
150
Distance (mm)

Fig. 4.

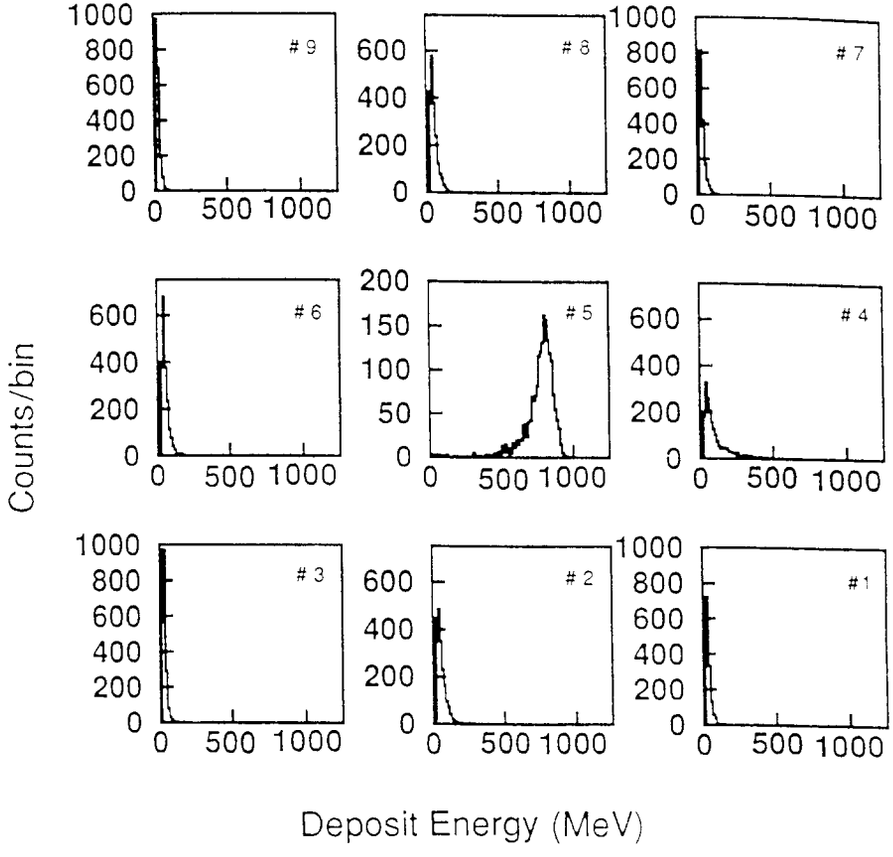
#9
#8
#7
#6
#5
#4
#3
#2
#1
Counts/bin
Deposit Energy (MeV)

Fig. 5.

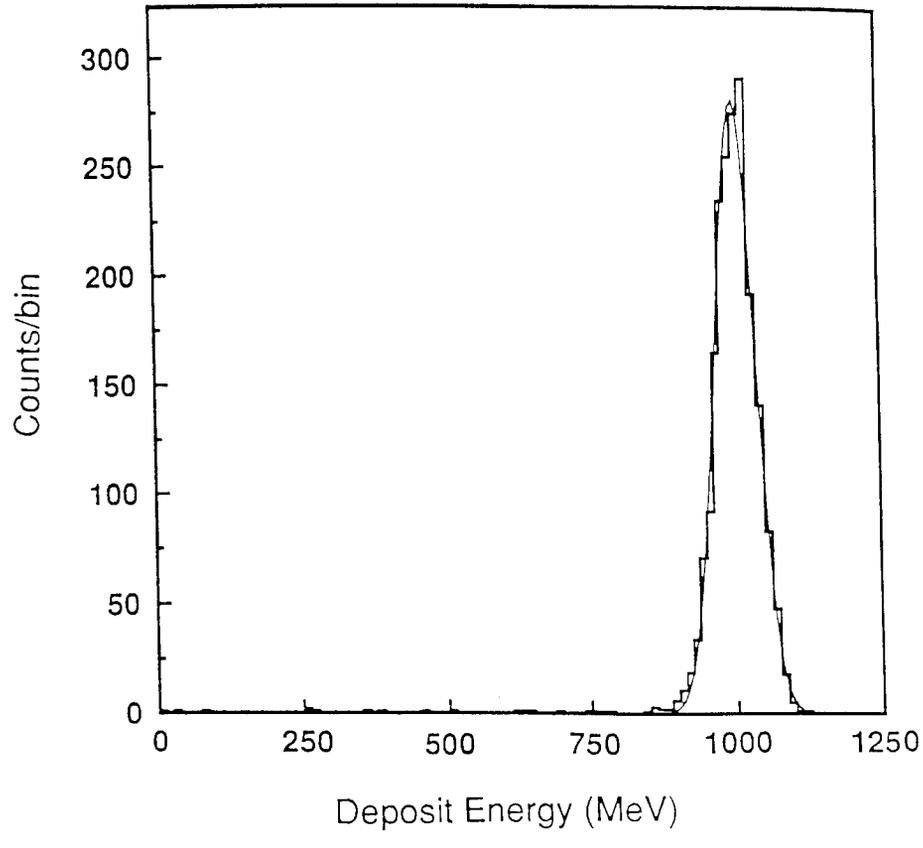
Counts/bin
Deposit Energy (MeV)

Fig. 6.

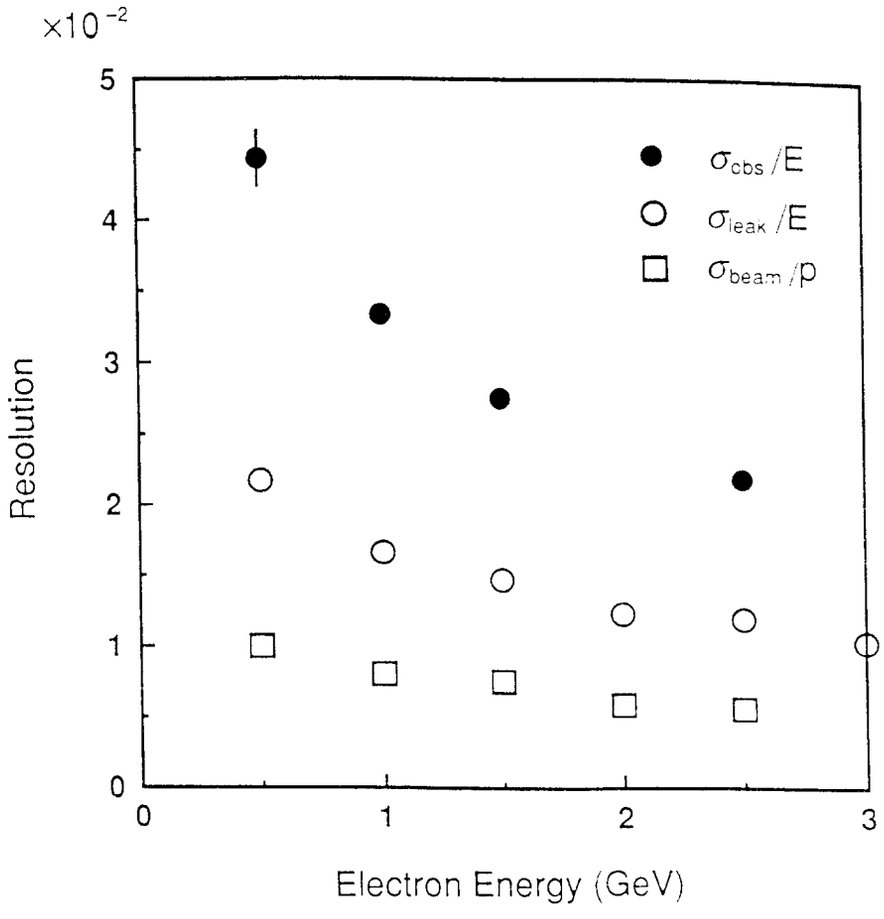
×10⁻²
Resolution
Electron Energy (GeV)
σcbs /E
σleak /E
σbeam /p
0
1
2
3
4
5

Fig. 7.

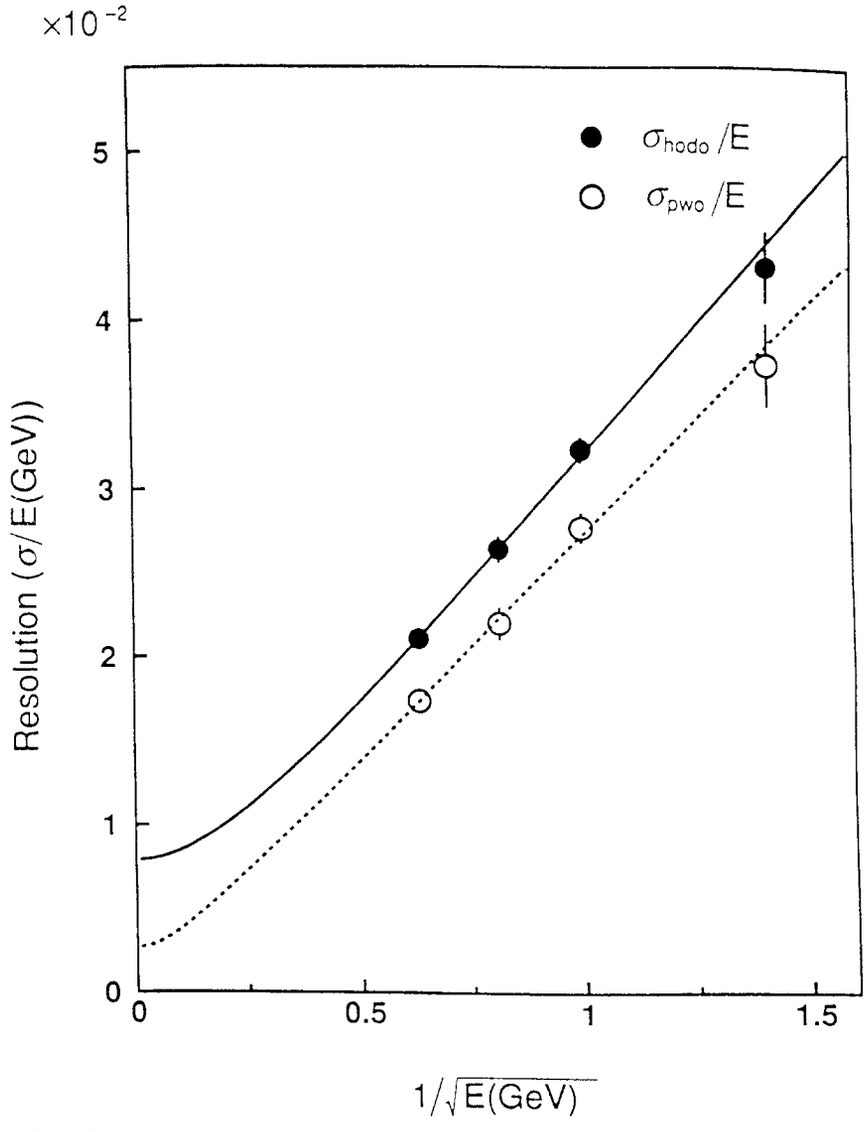
×10⁻²
Resolution (σ/E(GeV))
1/√E(GeV)
σhodo /E
σpwo /E
0
0.5
1
1.5
2
3
4
5

Fig. 8.

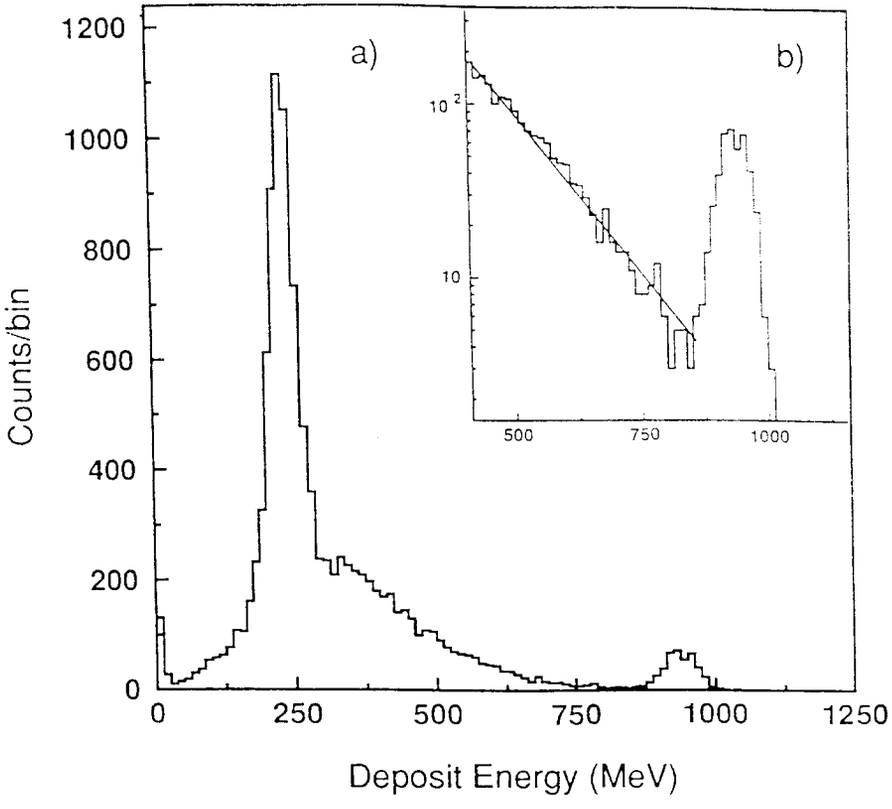
a)
b)
Counts/bin
Deposit Energy (MeV)
0
200
400
600
800
1000
1200
250
500
750
1000
1250
10^2
10
500
750
1000

Fig. 9.

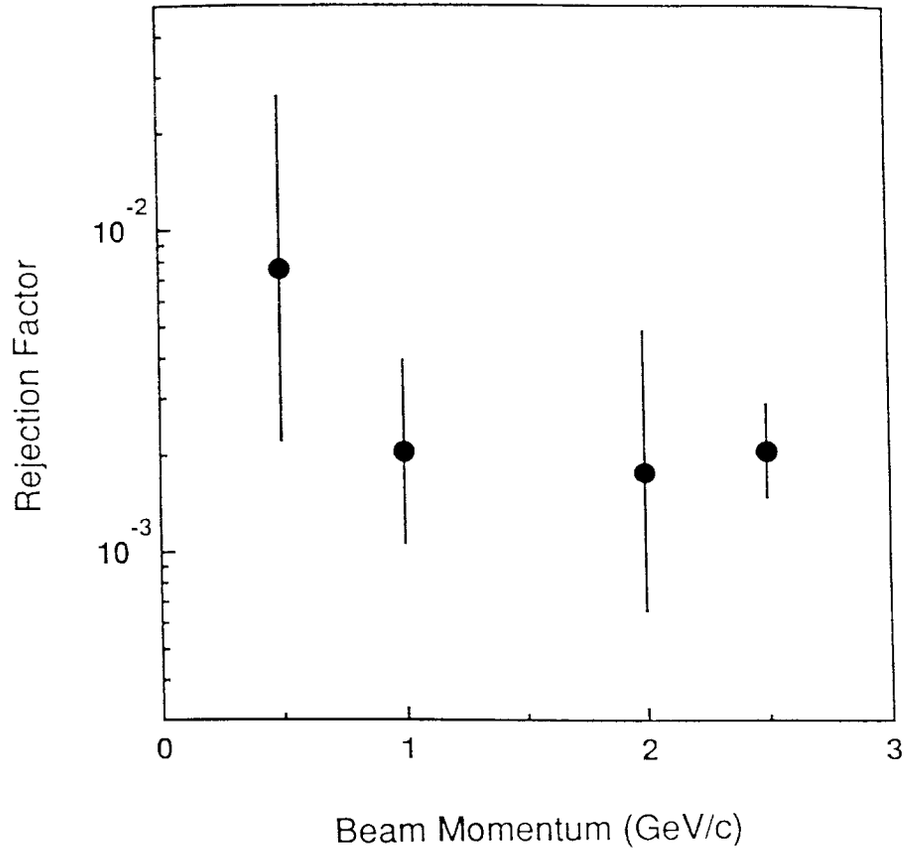
Rejection Factor
Beam Momentum (GeV/c)
10^{-2}
10^{-3}
0
1
2
3

Fig. 10.